JOURNAL OF MATERIALS SCIENCE: MATERIALS IN MEDICINE 3 (1992) 175–179

Hydroxyapatite coatings by a polymeric route

T. BRENDEL, A. ENGEL, C. RÜSSEL
Institut für Werkstoffwissenschaften III (Glas und Keramik), Universität Erlangen, Martensstr. 5, 852 Erlangen, Germany

A new polymeric route using calcium nitrate and phenyldichlorophosphine as initial compounds and acetone as solvent is described. Hydrolysis and subsequent oxidation with air led to the formation of a viscous solution which could be transformed to a solid polymer by subsequent drying. Calcining this polymer at temperatures in the range of 900 to 1100 °C led to the formation of hydroxyapatite possessing a slightly distorted lattice. Dip-coating of alumina and titanium substrates using highly viscous solutions, or repeatedly carried out dip-coating, led to the formation of thick, highly porous hydroxyapatite layers.

1. Introduction

On grounds of their chemical composition, which is roughly equivalent to the inorganic matrix of the human bone, calcium phosphates have been shown to be suitable materials for implants in orthopaedics and dentistry [1–3]. In the last few years, many attempts have been made in the preparation of hydroxyapatite, $Ca_{10}(PO_4)_6(OH)_2$, and other calcium phosphates with various preparation routes and precise characterization of the products obtained [4–13]. In contrast to metals or bioinert ceramics such as alumina, where an encapsulation with connective tissues takes place, hydroxyapatite is not only biocompatible like those, but also bioactive. This means that after implantation a direct bonding with the bone is realized [15–17].

Unfortunately, the mechanical strength of calcium phosphates is fairly poor and therefore, for many purposes, bulk materials cannot be used as implants [14]. In order to obtain bioactive materials with high mechanical strength, usually metal implants or alumina are coated with a thin layer of hydroxyapatite [18–20]. Up to now, this could be solely achieved by plasma spray techniques. The main problem associated with this technique is the lack of an exact stoichiometry and the occurrence of glassy phases in the ceramic layer. Some of these additional phases do not show a bioactive behaviour or are dissolved in the biological environment. Sol–gel techniques, in principle, also enable the formation of thin layers, but due to the volatility of the alkoxy phosphorus compounds used, an exact stoichiometry can scarcely be achieved. In this paper, a new polymeric route is described enabling the formation of hydroxyapatite layers with exact stoichiometry.

2. Experimental procedure

Phenyldichlorophosphine, $C_6H_5PCl_2$ (Strem Chemicals), was mixed with acetone and carefully hydrolysed with water. Due to the highly exothermic hydrolytic reaction, the temperature increased during this procedure to a value of around 45 °C. After cooling to room temperature, a solution of an exact stoichiometric quantity of calcium nitrate, $Ca(NO_3)_2 \cdot 4H_2O$ in acetone was added. Then the solution was oxidized by bubbling with air. After 1 h, a considerable increase in viscosity was observed.

For the preparation of bulk material, the solution was heated up to around 50 °C in order to vaporize the solvent. After 1 h, a yellow-coloured fluid possessing gel-like consistency was obtained. Further heating to 70 °C led to the formation of a polymeric foam and the evaporation of nitric gases. The polymer was dried at 100 °C and subsequently calcined at temperatures in the range of 400 to 1200 °C in air.

Substrates of alumina, metallic titanium or titanium alloys were dip-coated with the viscous solution. Alumina substrates were thermally pre-treated at temperatures in the range of 1200 to 1300 °C. The layers formed were dried and subsequently calcined (heating rate: 1 K min^{-1} up to temperatures of 500 °C, at higher temperatures: 100 K h^{-1}) in a vacuum (metallic titanium or alloys) or in air (alumina).

The intermediates and products obtained were characterized using X-ray diffraction (XRD) (Siemens D 500, for the characterization of the coatings a thin film accessory was used) ($CuK_\alpha = 0.154$ pm), Fourier transform infrared spectroscopy (FTIR) (Mattson Polaris), thermogravimetry (TGA) (Netzsch STA 409, applied heating rate: 2 K min^{-1}) and scanning electron microscopy (SEM) (Cambridge). The bulk material was further characterized by chemical analysis, using an inductive coupled plasma (ICP) (Leeman Labs 2.5). The mean grain size was determined by laser granulometry (Cilas 715).

3. Results and discussion

Fig. 1, graph (a) shows the FTIR spectrum of a solution of phenyldichlorophosphine in acetone, while graph (b) represents the same solution after the addition of water. Besides lines related to the solvent acetone at 530, 1090, 1370, 1420, 1720 cm^{-1} and in the range of 2980–3010 cm^{-1}, lines related to the phenyl group ($\nu_{C=C}$: 1600 cm^{-1}, $\delta_{C\text{-}Hoop}$ (oop: out of plane),

0957–4530

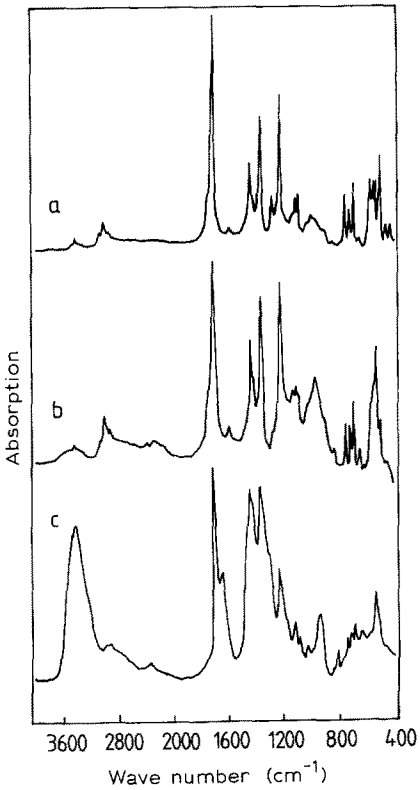

Figure 1 FTIR spectra of (a) phenyldichlorophosphine + acetone, (b) phenyldichlorophosphine + acetone + water, (c) viscous solution.

δ_{ring}: 690–750 cm^{-1}) and phosphorus–phenyl vibrations (1130 cm^{-1}) can be seen in both spectra. In addition, graph (a) shows two lines at 420 and 440 cm^{-1} due to phosphorus–chlorine bonds. During hydrolysis these lines disappeared and a broad P–O line at 900 to 1050 cm^{-1} was observed. In coincidence with the observation of a drastic temperature increase, the corresponding chemical reaction is described by

$$C_6H_5\text{–}PCl_2 + H_2O \rightarrow C_6H_5\text{–}P(OH)_2 + 2HCl \quad (1)$$

Fig. 1, graph (c) shows an FTIR spectrum of the viscous solution. Besides lines related to the acetone and NO_3^- (broad lines at 1630 and 1300 to 1500 cm^{-1}), phosphorus–phenyl bonds, lines due to the phenyl group and lines related to P=O bonds (1130 cm^{-1}) as well as a broad absorption due to P–O–P bonds (900–980 cm^{-1}) can be seen. The chemical reactions during the oxidation with air and subsequent vaporization of water and solvent are therefore suggested to be as follows:

$$C_6H_5\text{–}P(OH)_2 \xrightarrow[-H_2O]{+O_2} \text{—P(O)(}C_6H_5\text{)—O—P(O)(}C_6H_5\text{)—O—P(O)(}C_6H_5\text{)—O—P(O)(}C_6H_5\text{)—O—} \quad (2)$$

Drying the viscous solution led to a decrease of the bonds related to the solvent.

Fig. 2 shows a TGA profile of the dried polymeric compound. About 4% weight loss was observed at a temperature of around 150 °C, considerable weight

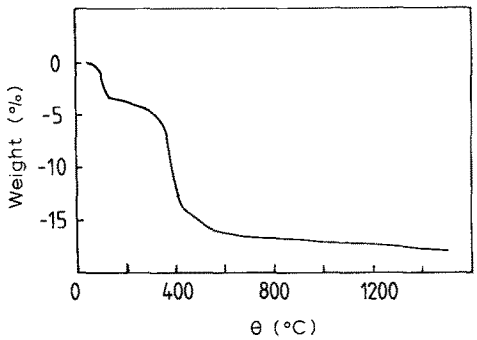

Figure 2 TGA profile of a dried polymer (heating rate: 2 K min^{-1}).

loss of about 10% was seen at temperatures in the range of 350 to 400 °C, and a further slight weight loss even at temperatures above 800 °C. The ceramic yield was about 82%. Simultaneously recorded differential thermal analysis (DTA) profiles show that the reaction in the range of 350 to 400 °C was highly exothermic; another, relatively broad, exothermic peak was observed in the range of 600 to 850 °C.

Fig. 3 shows FTIR spectra of samples calcined at different temperatures. At a calcination temperature of 350 °C, some lines due to the δ-phenyl vibrations at around 690 to 750 cm^{-1}, and a broad absorption at around 500 to 600 cm^{-1} due to the phosphorus–phenyl vibration, and considerable absorption at 1430 to 1620 cm^{-1} due to NO_3^- can be seen. Lines related to P=O and P–O can be observed at 1100 and 900 cm^{-1}, respectively. At a calcination temperature of 400 °C, absorptions due to P–O deformation and P–O valence vibrations are much stronger and considerably sharper while the intensity of lines related to the phenyl group decreased drastically. FTIR spectra of samples calcined at 1000 °C match those recorded from commercially available hydroxyapatite. The sharp lines at 3500 and at 620 cm^{-1} are due to non-bridging O–H. At calcination temperatures higher than 1000 °C, the intensity of these lines decreased again, due to the evaporation of crystal water. The spectra recorded from samples calcined at 400 and 1000 °C are fairly similar, but some organic groups can still be seen from the sample calcined at 400 °C. This is in agreement with the observed colours of the calcined samples. The initial polymer has a yellow colour, slight darkening can be observed at a calcination temperature of 300 °C, while samples calcined at 350 °C possess a dark brownish colour. Calcining at temperatures in the range of 390 to 500 °C led to greyish samples, while at 700 and 850 °C, slightly grey and white samples are obtained, respectively.

Fig. 4, graph (a) shows an XRD pattern of the polymeric precursor which is completely amorphous.

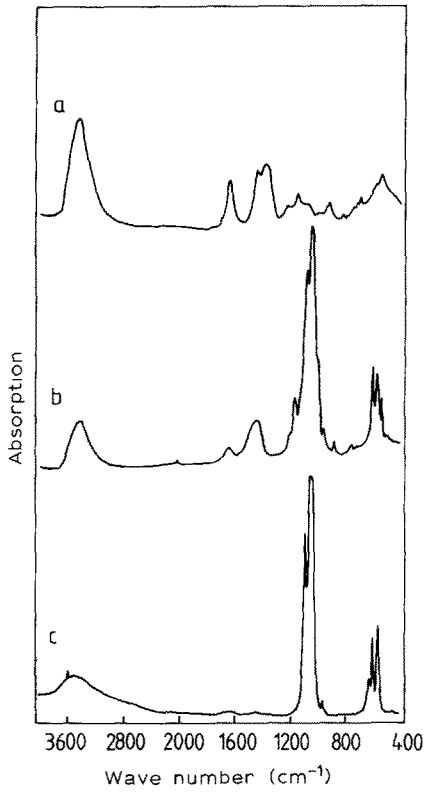

Figure 3 FTIR spectra of sample calcined at (a) 350 °C, (b) 400 °C, (c) 1000 °C.

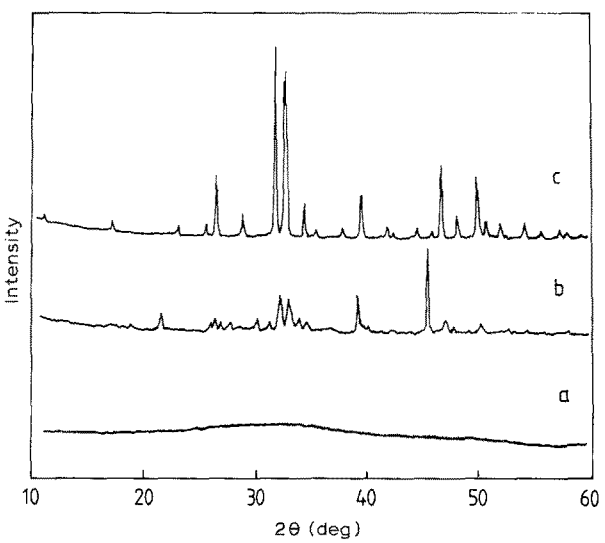

Figure 4 XRD patterns of (a) dried polymer, (b) sample calcined at 400 °C, (c) sample calcined at 1100 °C.

Amorphous products are also obtained at calcination temperatures up to 350 °C. Graph (b) shows that a sample calcined at 400 °C is crystalline, while calcination at 1100 °C led to a product possessing XRD lines approximately matching those of commercially available hydroxyapatite, but it should be noted that graph (b) shows some similarities to the XRD patterns of hydroxyapatite.

Samples dried at 200 °C and subsequently calcined deliver a ceramic yield of around 86%. Since at the end of the calcination process hydroxyapatite is formed, the stoichiometry related to the phosphorus/calcium ratio remains constant during calcination. It can be concluded that volatile phosphorus compounds are not formed during calcination, as additionally proved by chemical analysis of calcined samples. At temperatures in the range of 350 to 400 °C, the main weight loss is observed and the main quantity of organic compounds is removed in an exothermic reaction. At temperatures above 800 °C the organics are completely burnt out, and further weight loss at higher temperatures is due to the evaporation of crystal water as shown by FTIR spectroscopy. Since the total weight loss of samples previously dried at 200 °C is only 14%, the dried precursor contains only relatively small amounts of organic compounds and only minor quantities of nitrogen compounds (the calcium-containing starting material was $Ca(NO_3)_2$). Assuming that the phenyl–phosphorus bond is not destroyed during drying at 200 °C, the compound possessing the minimum quantity of organic with the given phosphorus/calcium stoichiometry is $6\,PO_2C_6H_5 \cdot 10\,CaO$:

$$6\,PO_2C_6H_5 \cdot 10\,CaO \xrightarrow[-\text{organic}]{+O_2} Ca_{10}(PO_4)_6(OH)_2 \quad (3)$$

The total weight loss of 14.5% calculated from Equation 3 is in fairly good agreement with the observed weight loss of 14%, but it should be mentioned that the chemical formula of the polymeric precursor is only an extremely simplified description and not in total agreement with the FTIR spectra.

Fig. 5 shows XRD patterns of samples calcined at different temperatures in the range of 900 to 1100 °C. It can be seen that the lines are considerably shifted. The higher the calcination temperature, the better the agreement with the XRD patterns of commercially

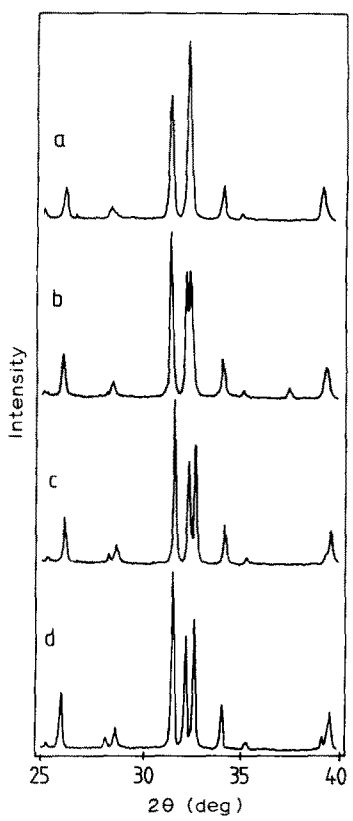

Figure 5 XRD patterns of calcined samples: (a) 900 °C, 2 h soaking time; (b) 900 °C, 10 h soaking time; (c) 1000 °C, 10 h soaking time; (d) 1100 °C, 10 h soaking time.

available hydroxyapatite. In Fig. 5 the lines are shown together with their Miller (hkl) indices. At lower calcination temperatures, lines possessing high l indices and low h and k indices are shifted toward higher 2θ values, while those possessing low l indices and high h and k indices are shifted to lower 2θ values. Therefore, it can be concluded that the hydroxyapatite lattice is more distorted at lower calcination temperatures. The lattice constants of samples calcined at 900 °C, applying a soaking time of 2 h, can be calculated to be 956.0 and 679.4 pm for a_0 and c_0, respectively. By comparison, the lattice constants of commercially available hydroxyapatite, a_0 and c_0, are 941.8 and 688.4, respectively. Table I summarizes the lattice constants of products calcined at different temperatures and those of commercially available hydroxyapatite.

It should be mentioned that additional phases such as tricalcium phosphate, tetracalcium phosphate or calcium oxide have never been observed.

Fig. 6 shows an SEM micrograph of hydroxyapatite powder calcined at 1100 °C. Fairly small and spherical particles can be seen; some of them are in the submicrometre range and slight agglomeration is observed. A mean particle size of 0.9 μm was determined by laser granulometry.

Fig. 7 shows an SEM micrograph of an alumina substrate dip-coated with the viscous solution and calcined at 1100 °C. The layer is fairly porous and possesses a thickness of around 25 μm. Fig. 8 shows an SEM micrograph of an alumina substrate with a thin coating. The layer is fairly homogeneous and possesses a layer thickness smaller than 1 μm. Only some small cracks, predominantly in the triple points of the alumina substrates, can be seen.

TABLE I Lattice constants a_0 and c_0 of hydroxyapatite bulk material calcined at different temperatures

Sample calcination temperature/soaking time	Lattice constants (pm)	
	a_0	c_0
900 °C/2 h	956.0	679.4
900 °C/10 h	954.0	681.7
1000 °C/10 h	949.1	680.7
1100 °C/10 h	948.8	684.0
Commercial product	941.8	688.4

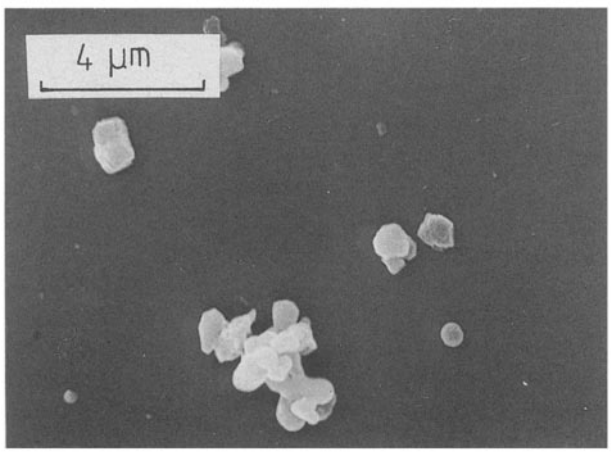

Figure 6 SEM micrograph of powder calcined at 1100 °C.

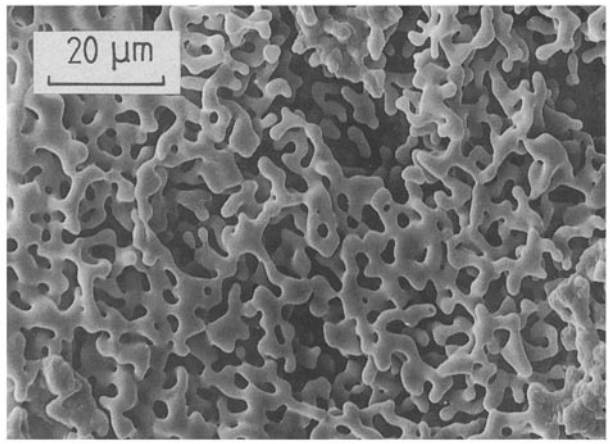

Figure 7 SEM micrograph of thick and porous hydroxyapatite coating on an alumina substrate.

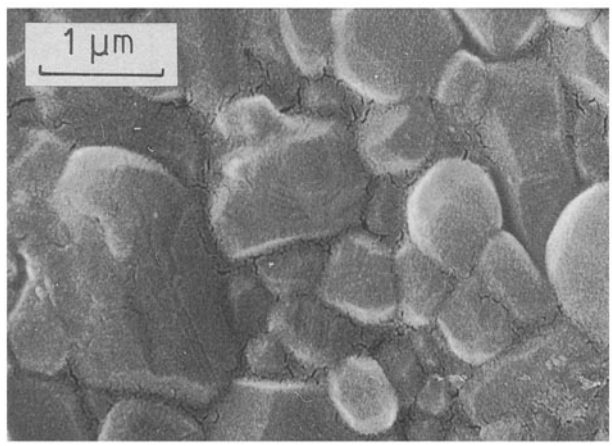

Figure 8 SEM micrograph of thin hydroxyapatite coating on an alumina substrate.

Titanium substrates exhibited nearly the same behaviour as alumina substrates. Fig. 9 shows an SEM micrograph of a coated titanium substrate. The sample was prepared by dip-coating and subsequent calcining at 1100 °C in a vacuum. Then a second dip-coating procedure was carried out and the sample was calcined again at 1100 °C. The coating obtained was fairly thick (~ 2 μm) and porous, but large cracks could not be observed.

XRD patterns of fairly thick coatings showed only lines related to the desired product, hydroxyapatite, while thin coatings showed additional lines. Titanium substrates also delivered lines related to TiO_2 and to tricalcium phosphate. It is supposed that this is due to a chemical reaction at the interface titanium oxide–hydroxyapatite, possibly leading to the formation of $CaTiO_3$ which, however, could not be detected. XRD patterns of alumina substrates with thin coatings also showed additional phases: besides alumina and hydroxyapatite, tricalcium phosphate could be detected. The stoichiometry of the layer was therefore shifted towards a lower calcium content and it should be assumed that this is due to the formation of $CaO \cdot xAl_2O_3$ compounds which, however, also in this case could not be detected by XRD.

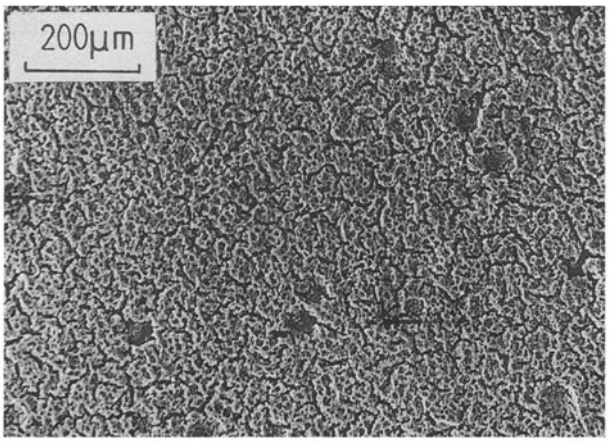

Figure 9 SEM micrograph of hydroxyapatite coating on metallic titanium.

The calcium/phosphorus ratio in the case of hydroxyapatite is 1.67 while it is 1.5 for tricalcium phosphate. This demonstrates that both values are fairly close to each other. If hydroxyapatite reacted at the interface with alumina and, besides $CaO \cdot xAl_2O_3$ compounds, equal quantities of tricalcium phosphate and hydroxyapatite were formed, only around 5% of the total quantity of calcium in the hydroxyapatite would be removed to form $CaO \cdot xAl_2O_3$ compounds. It is fairly obvious that this small amount of $CaO \cdot xAl_2O_3$ compounds may not be detected by XRD, especially because thin films are investigated. Fairly similar considerations should be valid for the formation of $CaTiO_3$ in the case of titanium substrates. Another hint, in the case of chemical reactions at the interface being responsible for the formation of tricalcium phosphate, is the observation that the quantity of tricalcium phosphate formed depends on the type of alumina substrate used. If alumina of high purity (99.6% Al_2O_3, rest: MgO) with only a negligible amount of glassy phase was used, the ratio hydroxyapatite/tricalcium phosphate was around 2.3:1, while using alumina substrates with a high amount of glassy phase ($\sim$ 3%), the hydroxyapatite/tricalcium phosphate ratio was around 1:2.3. Supposedly the glassy phase promotes the decomposition of hydroxyapatite due to the thermodynamically advantageous formation of calcium-containing glassy phases.

4. Conclusions

A new polymeric route, using phenyldichlorophosphine and calcium nitrate as starting materials, enables the formation of exactly stoichiometric hydroxyapatite which shows, as far as it can be detected by XRD, no additional phases such as tricalcium phosphate. Dip-coating of substrates using viscous precursor solutions and subsequent drying and calcining enables the formation of thin and nearly fully dense coatings whose XRD patterns indicated the presence of hydroxyapatite as well as of tricalcium phosphate. Dip-coating using more viscous solutions, or repeated dip-coating, led to the formation of thick, highly porous hydroxyapatite layers.

References

1. J. F. OSBORN, "Implantatwerkstoff Hydroxylapatit" (Quintessenz, Berlin, 1985).
2. K. de GROOT, in "Ceramics in Surgery", edited by P. Vincenzini (Elsevier, Amsterdam, 1983) p. 79.
3. *Idem, Biomater.* **1** (1980) 47.
4. J. G. J. PEELEN, B. V. REJDA and K. de GROOT, *Ceram. Int.* **4** (1978) 71.
5. M. JARCHO, C. H. BOOLEN, M. B. THOMAS, J. BOBICK, J. F. KAY and R. H. DOREMUS, *J. Mater. Sci.* **11** (1976) 2027.
6. G. BONEL, J.-C. HEUGHEBAERT, M. HEUGHEBAERT, J. L. LACOUT and A. LEBUGLE, in: Annals of the New York Academy of Science, Vol. 523, edited by P. Ducheyne and J. Lemons (1988) p. 115.
7. T. HATTORI and Y. IWADATE, *J. Amer. Ceram. Soc.* **73** (1990) 1803.
8. T. KIJIMA and M. TSUTSUMI, *ibid.* **62** (1979) 455.
9. K. UEMATSU, M. TAKAGI, T. HONDA, N. UCHIDA and K. SAITO, *ibid.* **69** (1986) 590.
10. N. YAMASAKI, T. KAI, M. NISHIOKA, K. YANAGISAWA and K. JOKU, *J. Mater. Sci. Lett.* **9** (1990) 1150.
11. E. G. NORDSTRÖM and K. H. KARLSSON, *J. Mater. Sci: Mater. Medicine* **1** (1990) 182.
12. A. KRAJEWSKI, A. RAVAGLIOLI, N. ROVERI, A. BIGI and E. FORESTI, *J. Mater. Sci.* **25** (1990) 3203.
13. N. YAMASHITA, H. OWADA, H. NAKAGAWA, T. UMEGAKI and T. KANAZAWA, *J. Amer. Ceram. Soc.* **69** (1986) 590.
14. T. KANAZAWA, T. UMEGAKI, K. YAMASHITA, H. MONMA and T. HIRAMATSU, *J. Mater. Sci.* **26** (1991) 417.
15. B. M. TRACY and R. H. DOREMUS, *J. Biomed. Mater. Res.* **18** (1984) 719.
16. G. L. de LANGE and K. DONATH, *Biomater.* **10** (1989) 121.
17. G. L. de LANGE, C. de PUTTER, K. de GROOT and E. H. BURGER, *J. Dent. Res.* **68** (1989) 509.
18. W. R. LANCEFIELD, in: Annals of the New York Academy of Science, Vol. 523, edited by P. Ducheyne and J. Lemons (1988) p. 72.
19. M. AKAO, H. AOKI and K. KATO, *J. Mater. Sci.* **16** (1981) 809.
20. F. B. BAGAMBISA, *ibid.* **25** (1990) 5091.

Received 5 April
and accepted 1 May 1991